3

Characteristics of Biochar: Microchemical Properties

James E. Amonette and Stephen Joseph

Introduction and scope

Biochars, being derived from a variety of biological feedstocks that have been thermally degraded under a range of conditions (Chapter 8), exhibit a correspondingly large range in composition and chemistry. Due, in part, to the complex set of chemical reactions that occur during thermal processing, a large degree of chemical heterogeneity extends to the microscopic scale, even within a single biochar. Thus, in the strictest sense, each biochar made with a particular feedstock and process combination presents a unique mixture of phases and microenvironments that gives rise to a unique set of chemical properties. In some respects, the chemical complexity of biochars rivals that of incipient soils. In this chapter we focus on the chemical complexity of biochar as manifested primarily at a microscopic and molecular scale. We start by describing the biochar-formation process and how this influences the composition and nature of the solid phases, entrained oils and their organization at the microscopic level. We then proceed to discuss the range of surface chemistries exhibited by biochars in terms of functional groups and electrochemical properties. We conclude with a discussion of the influence of these properties on the sorption of aqueous species at biochar surfaces.

Formation and bulk composition

Formation

When biological material is thermally degraded in sub-stoichiometric oxygen (O) conditions, it yields a solid residue. The various definitions for this solid residue are given in Chapter 7.

A number of feedstocks and thermal degradation processes can be used to produce biochar. Potential feedstocks include all materials of biological (organic) origin,

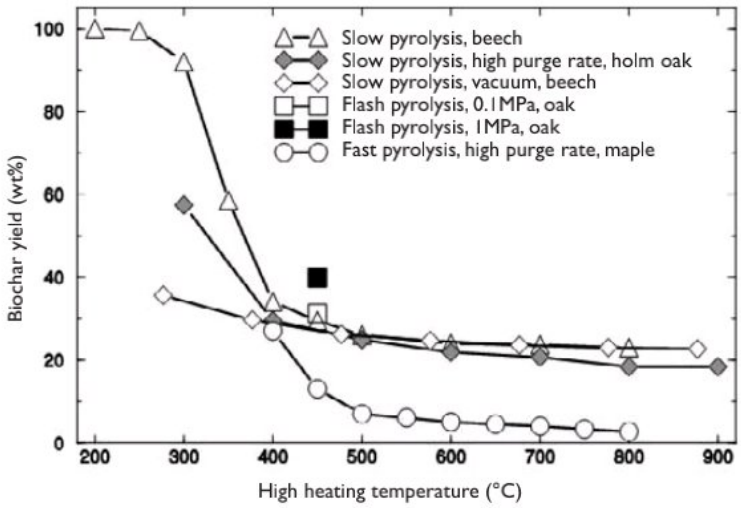

Figure 3.1 *Biochar yields for wood feedstock under different pyrolysis conditions*

Source: slow pyrolysis data from Schenkel (1999) as presented by Antal and Grønli (2003) (beech); Figueiredo et al (1989) (high purge rate, holm oak); and Demirbas (2001) (vacuum, beech). Flash pyrolysis data from Antal et al (2000) (oak). Fast pyrolysis data from Scott et al (1988) (eastern red maple).

such as manures, rendering wastes, and lignocellulosic biomass. The latter is an obvious choice as the primary feedstock because it is the most abundant biologically produced material. Thermal degradation processes include hydrothermal conversion, torrefaction, slow pyrolysis, fast pyrolysis, gasification and various permutations (Chapter 8). They are distinguished chiefly by the presence or absence of free water, feedstock residence time, availability of atmospheric O_2, heating rate, gas environment (e.g. the presence of nitrogen (N) or steam), and the temperatures and pressures used. The pyrolysis and gasification processes are described in detail in Chapter 8. Hydrothermal conversion occurs when feedstock, immersed in water, is heated at temperatures of 180°C to 250°C in a sealed vessel at autogenous pressure (0.5MPa to 1MPa) for periods of several hours to a day in length (Titirici et al, 2007a). Torrefaction involves heating the feedstock to temperatures of 200°C to 300°C at slow heating rates (<50°C min^{-1}) under an anoxic atmosphere at near-ambient pressure (Tito Ferro et al, 2004; Bergman and Kiel, 2005). Because most thermal degradation of biomass for biochar production currently involves the pyrolysis process, our discussion of the chemical aspects of biochar formation will focus on this process.

Pyrolysis of dry lignocellulosic materials involves three major parallel pathways (Shafizadeh, 1982; Varhegyi et al, 1994; Antal and Grønli, 2003):

1 a biochar- and gas-forming pathway;
2 a liquid- and tar-forming pathway; and
3 a gasification and carbonization pathway.

Competition between these pathways, whose relative rates are largely determined by the highest heat treatment temperature (HTT), volatile removal rate and particle residence time encountered during the process, controls the relative abundance of the thermal-degradation products (see Figure 3.1). In this section, we provide an overview of the chemistry occurring during the biochar-formation process, drawn, except where noted, from the reviews of Shafizadeh (1982) and Antal and Grønli (2003).

Lignocellulose degradation begins at temperatures above approximately 120°C and is dominated by the biochar- and gas-formation pathway at HTTs below 300°C. This pathway is believed to be a free-radical process initiated by homolytic cleavage of bonds. The free radicals that drive the process are initially formed by thermal action on structural O and inorganic impurities present in the feedstock. An additional source

of free radicals may be from low levels of atmospheric O_2 that may be present during the initial stages of pyrolysis. Carboxyl and carbonyl groups are formed and subsequently cleaved to yield CO_2 and CO (Shafizadeh, 1982; Brennan et al, 2001). Water is also released as a result of dehydration reactions. Ultimately, some of the free-radical fragments recombine in various ways with each other and with the substrate to yield a biochar residue.

At HTTs of between 300°C and about 600°C, a different liquid- and tar-forming pathway becomes increasingly important. As a result, biochar production decreases significantly over this temperature range. The tar that is produced from cellulose is chiefly composed of anhydrosugars such as levoglucosan that are less reactive than the free-radicals generated by homolytic bond cleavage (Shafizadeh, 1982). Because of increased heat- and mass-transfer rates at these HTTs, volatilization of the anhydrosugars is also possible, thus further decreasing the potential for biochar formation. In lieu of volatilization, however, the anhydrosugars can be degraded by dehydration and fission reactions that are promoted by acidic or basic catalysts. Subsequent homolytic bond cleavage of the secondary products yields biochar. The proportion of free radicals trapped in the biochar as measured by electron paramagnetic resonance (EPR) spectroscopy also increases with HTT for a given residence time and reaches a maximum at HTTs of 500°C to 600°C (Bradbury and Shafizadeh, 1980; Degroot and Shafizadeh, 1983; Feng et al, 2004). As a result, biochars produced in this temperature range are extremely reactive towards oxidation (usually measured by O_2 chemisorption), often to the point of being pyrophoric. In general, the amount of biochar produced at HTTs of 300°C to 600°C, while substantially less than that at lower HTTs, depends largely upon the relative rates of volatilization and degradation of the anhydrosugars present in the tar. As heat- and mass-transfer rates (i.e. volatilization) increase, the yields of biochar decrease.

At HTTs above 600°C, heat- and mass-transfer rates are sufficiently high that a gas-forming pathway dominates, and biochar, tar and liquid formation are at a minimum. The biochar that forms initially as the substrate is being heated is carbonized, by which process more of the original O, hydrogen (H), N and sulphur (S) are removed and carbon (C) contents above 90 per cent by weight are readily obtained (Chapter 4). The number of trapped free radicals in the biochar measured by EPR spectroscopy also decreases due to defect-annealing processes at the higher temperatures (Bradbury and Shafizadeh, 1980; Feng et al, 2004), although some evidence suggests that the decrease is due to the location at the biochar surface of a greater proportion of the free radicals generated where they may react with chemisorbed O_2 and quench the EPR signal (Degroot and Shafizadeh, 1983).

Although we have focused on the primary role played by HTT, the proportion of the feedstock that is converted to biochar during pyrolysis also depends upon heating rate (inversely proportional to residence time), gas purge rate, pressure and feedstock composition. In general, lower HTTs, slower heating and purge rates, higher pressures, and greater concentrations of lignin in the substrate result in larger yields of biochar (Shafizadeh, 1982; Demirbas, 2001; Antal and Grønli, 2003).

Solid phases and their distribution

As described above, process conditions (chiefly temperature and heating rate) may cause a significant fraction of the initial carbonaceous material to be released as oily and tarry vapours during thermal degradation. At low HTTs (i.e. below 500°C), some of these vapours condense in the pores of the

biochar, leading to a multi-phase substance (Schnitzer et al, 2007a, 2007b), while the majority are commonly recovered from the gas stream as bio-oil using a condensation tower. Inorganic compounds present in the feedstock undergo a similar process, with some being volatilized during thermal degradation (see Chapter 5), and the majority being retained either as discrete mineral phases or as part of the structure of the carbonaceous residue (Wornat et al, 1995).

Carbon-based phases

Several researchers have described the evolving nature of the carbonaceous residue obtained when lignocellulosic biomass is thermally degraded under various conditions (Antal and Grønli, 2003; Kercher and Nagle, 2003; Paris et al, 2005; Skodras et al, 2006; Stresov et al, 2007). As described by Paris et al (2005), four regions of change (dehydration, pyrolysis, graphene nucleation and carbonization) are observed under non-hydrothermal conditions. With very slow heating rates (approximately 2°C min^{-1}; Paris et al, 2005) and near-ambient pressure, transitions between these regions occur at about 250°C, 350°C and 600°C. At faster heating rates, these transitions occur at higher temperatures due to heat- and mass-transfer limitations. In the first region (i.e. at temperatures below 250°C), the primary changes in the feedstock are dehydration and slight depolymerization of cellulose. Little mass loss is observed. Between 250°C and 350°C, complete depolymerization (pyrolysis) of the cellulose occurs, resulting in significant mass loss by volatilization and creation of an essentially amorphous C matrix. At about 330°C, the first signs of aromatic C are seen, and above 350°C, polyaromatic graphene sheets begin to grow at the expense of the amorphous-C matrix. Above 600°C, carbonization begins, by which most of the remaining non-C atoms are removed and graphene sheets continue to grow laterally, eventually coalescing.

From a compositional standpoint, the major constituents of biomass (C, H and O) volatilize during dehydration and pyrolysis (see Chapter 4), with H and O being lost in proportionally greater amounts than C. The O and H are lost initially as water, and later as hydrocarbons, tarry vapours, H_2, CO and CO_2 (Antal and Grønli, 2003). The proportion of C in the solid phase increases from about 40 to 50 per cent by weight in the feedstock to on the order of 70 to 80 per cent by weight after pyrolysis between 250°C and 600°C. Carbonization further increases the C content to more than 90 per cent by weight except for high mineral-ash chars (Antal and Grønli, 2003).

The microstructural changes occurring during thermal degradation can be detected by a number of techniques, including transmission electron microscopy (TEM), infrared and Raman spectroscopies, electron energy loss spectroscopy (EELS), X-ray diffraction (XRD), and small-angle X-ray scattering (SAXS). The entire range of these changes is shown in SAXS patterns collected by Paris et al (2005) for slow pyrolysis of normal wood in which the initial feedstock structural features give way to a featureless profile at about 330°C, which is subsequently replaced by a new profile as the graphene sheets nucleate and coalesce at higher temperatures (see Figure 3.2).

As suggested by the extended transition from a purely amorphous C phase to one in which graphene sheets nucleate and grow, biochars produced at higher HTTs and carbonized biochars consist primarily of an intimate mixture of two solid C phases (i.e. amorphous C and graphene packets; see Chapter 2). This was first shown by Franklin (1951) using X-ray diffraction and has since been confirmed numerous times by using various structural and microscopic methods. A recent confirmation is provided by Cohen-Ofri et al (2006, 2007) using TEM (see Figure 3.3).

Building upon the work of Franklin

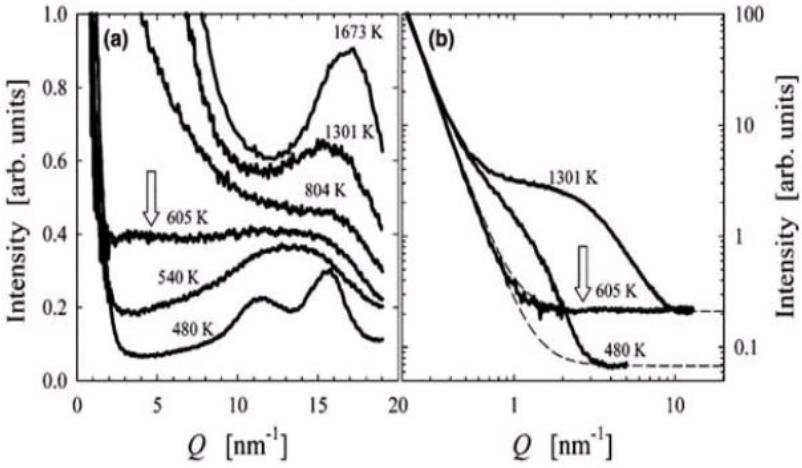

Figure 3.2 *Selected small-angle X-ray scattering (SAXS) profiles from normal wood: (a) the intensity is plotted versus the length of the scattering vector in a linear representation; and (b) for three selected profiles in a double logarithmic representation*

Note: The arrows emphasize the profile at T = 605K (330°C), which marks the almost structureless transition region between cellulose degradation and biochar formation.

Source: Reprinted from Paris et al (2005) with permission from Elsevier

(1951), a detailed quasi-percolation model describing the evolution of the graphene packets during carbonization at temperatures as high as 1400°C was developed by Kercher and Nagle (2003) using X-ray diffraction, which was supported through further observations by Paris et al (2005). The essential features of the model (see Figure 3.4) are that the number of graphene packets and their thickness remain constant as carbonization proceeds. They grow laterally at the expense of the amorphous C phase and eventually intersect with adjacent packets to provide electrical continuity through the biochar. Because the amorphous C is less dense than the aligned graphene packets, conversion creates voids in the structure, which increases the microporosity.

An analogous structural model for biochars carbonized at 950°C was presented by Bourke et al (2007). This model differed slightly from that of Kercher and Nagle (2003) by including non-graphitic rings interspersed in the nominally graphene sheets (i.e. 70 per cent aromaticity rather than 100 per cent), as well as the presence of larger multi-ring voids in the sheets. They further limited the graphene crystallite sizes in all dimensions to about 2nm, whereas Kercher and Nagle (2003) proposed packets that were more than 4nm thick and could extend laterally as far as 8.4nm.

In contrast to the relatively well-understood evolution and microstructure of biochars produced by pyrolysis and carbonization, little is known about the

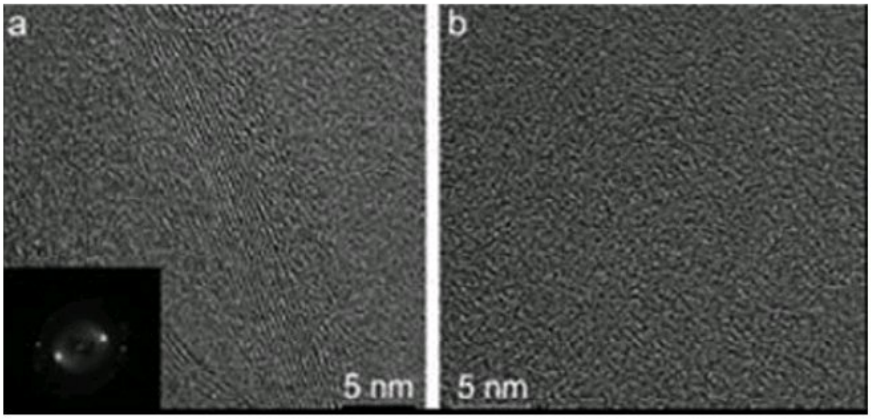

Figure 3.3 *Transmission electron microscopy (TEM) images of modern biochar samples: (a) ceratonia that contains organized and non-organized phases (inset: fast Fourier transform (FFT) of the organized region); (b) non-organized phase of Ceratonia biochar*

Source: Cohen-Ofri et al (2007).

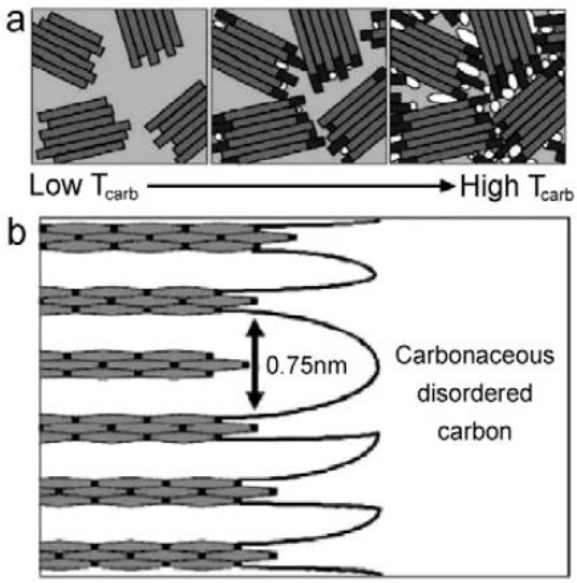

Figure 3.4 *Schematics demonstrating the concepts of the quasi-percolation model of Kercher and Nagle (2003): (a) light grey denotes the disordered carbon phase; medium grey denotes graphene sheets in large turbostratic crystallites present at low temperatures; dark grey denotes growth of the graphene sheets at higher temperatures, white denotes porosity; (b) fundamental concept of disordered C forms converting into high-density graphene sheets*

Note: In this simplistic example, the disordered C filling six graphene sheets' worth of volume can only convert into five graphene sheets' worth of material. The non-growing graphene sheet region becomes the beginning of a 0.75nm tall nanopore.

Source: reprinted from Kercher and Nagle (2003) with permission from Elsevier

conversion process and structure of biochars obtained under hydrothermal conditions (e.g. 180°C to 250°C, 0.5MPa to 1MPa). Antonietti and co-workers (Cui et al, 2006; Rothlein, 2006; Titirici et al, 2007a, 2007b) suggest that in the presence of an acidic catalyst, a 'coalification' process occurs by which water is removed from biomass to form a lignite-type product. As discussed by Titirici et al (2007a), the hydrothermal conversion approach essentially fixes the entire C into a solid phase that, similar to conventionally produced biochar, has significant potential for C sequestration because it is more stable than the original biomass from which it was formed. Although the process yields liquid intermediate products, essentially no liquid or tar remains when the process is carried to completion and the final solid is hydrophilic (Titirici et al, 2007a).

Entrained minerals

Two factors, feedstock and process conditions, control the amount and distribution of mineral matter in biochars. The mineral ash content of feedstocks varies significantly (see Table 3.1). Woody feedstocks generally have low (<1 per cent by weight) ash contents, whereas grass, straw and grain husks, which have high silica contents, may have as much as 24 per cent by weight ash (Raveendran et al, 1995). Much of the mineral content in the feedstock is carried over into the biochar where it is concentrated due to loss of C, H and O during pyrolysis (see Chapter 5). Biochars from manures and rendering wastes typically have very high ash contents. Chicken-litter biochars, for example, can have 45 per cent mineral matter (Koutcheiko et al, 2007), and bone biochars may have as much as 84 per cent mineral matter (Purevsuren et al, 2004).

The effect of feedstock mineral-ash content on biochar yield is uncertain. Amendments of solid catalysts such as alkali carbonates and NaCl to cellulose increase biochar yields (Feng et al, 2004). Addition of iron (Fe) to lignocellulosic feedstock has a similar effect (Edye et al, 1993). Removal of mineral content (i.e. demineralization) by pre-treatment with acidic, basic or chelating solutions decreases biochar yield (Raveendran et al, 1995). These observations seem to suggest that higher mineral-ash content in the feedstock tends to increase biochar yield. However, correlations between biochar yields and the mineral-ash content of various feedstocks that have not been amended with solid catalysts are weak to non-

Table 3.1 *Ash content and elemental composition of representative feedstocks and an oak wood biochar*

Feedstock	Ash content (wt %)	Al	Ca	Fe	Mg	Na	K	P	Si
					(mg kg^{-1})				
Bagasse	2.9	–[a]	1500	130	6300	90	2700	280	17,000
Coconut coir	0.8	150	480	190	530	1800	2400	50	3000
Coconut shell	0.7	70	1500	120	390	1200	2000	90	260
Coir pith	7.1	1700	3100	840	8100	11,000	26000	1200	13,000
Maize cob	2.8	–	180	20	1700	140	9400	450	9900
Maize stalks	6.8	1900	4700	520	5900	6500	30	2100	13,000
Cotton gin waste	5.4	–	3700	750	4900	1300	7100	740	13,000
Groundnut shell	5.9	3600	13,000	1100	3500	470	18,000	280	11,000
Millet husk	18.1	–	6300	1000	11,000	1400	3900	1300	150,000
Rice husk	23.5	–	1800	530	1600	130	9100	340	220,000
Rice straw	19.8	–	4800	200	6300	5100	5400	750	170,000
Subabul wood	0.9	–	6000	610	1200	90	610	100	200
Wheat straw	11.2	2500	7700	130	4300	7900	29,000	210	44,000
Olive kernel	2.6	18,000	97,000	24,000	20,000	7900	–	–	–
Almond shell	3.4	5000	80,000	6100	14,000	5500	–	–	–
Forest residue	1.2	4900	130,000	10,000	19,000	4200	–	–	–
Saw dust	0.44	9800	170,000	29,000	27,000	10,000	–	–	–
Waste wood	8.8	4900	130,000	10,000	19,000	4200	–	–	–
Willow wood	1.1	20	3900	30	360	150	1400	340	–
Demolition wood	1.9	480	3600	350	420	670	750	60	–
Straw	17.7	5800	8600	3400	3700	3200	22000	600	–
Meat and bonemeal	10.4	7600	260,000	4900	13,000	5800	23,000	100,000	–
Oak wood biochar	0.27	1000	350,000	3400	16,000	6400	98,000	5400	4200

Note: a No data reported.

Source: Raveendran et al (1995); Skodras et al (2006); and Bourke et al (2007) (oak biochar)

existent (see the data of Raveendran et al, 1995, for untreated feedstocks).

In addition to feedstock, process conditions, chiefly HTT, and the partial pressure of O_2, steam and carbon dioxide (CO_2) control the amounts of mineral ash in biochar (Bridgwater and Boocock, 2006). During thermal degradation, potassium (K) and chlorine (Cl) ions are highly mobile and will start to vaporize at relatively low temperatures (Yu et al, 2005). Calcium (Ca) is mainly located in cell walls and bound to organic acids (Marschner, 1995). Silicon (Si) is present in the cell walls as silica or as opal phytoliths (Marschner, 1995). Both Ca and Si are released during degradation at much higher temperatures than K and Cl (Bourke, 2006). Magnesium (Mg) is both ionically and covalently bonded with organic molecules and only vaporizes at high temperatures. Phosphorus (P) and sulphur (S) are associated with complex organic compounds within the cell and are relatively stable at low degradation temperatures (see Chapter 5). N is associated with a number of different organic molecules and can be released at relatively low temperatures (Schnitzer et al, 2007b). Other elements such as Fe and manganese (Mn) exist in a number of organic and inorganic forms in the biomass

and are largely retained during biochar formation (see Chapter 5).

Very little work has been carried out on the distribution and the stability of heavy metals in biochar. High mineral-ash biochars (especially chicken manure biochar and activated carbon) are known to adsorb heavy metals (Swiatkowski et al, 2004; Lima and Marshall, 2005).

Very little has been published on the distribution of mineral ash within different types of biochar. Of the inorganic elements that comprise mineral ash, most are believed to occur as discrete phases separate from the carbonaceous matrix. In some biochars, however, K and Ca are distributed throughout the matrix where they may form phenoxides (K, Ca) or simply be intercalated between graphene sheets (K) (Wornat et al, 1995).

Minerals found in biochars include sylvite (KCl), quartz (SiO_2), amorphous silica, calcite ($CaCO_3$), hydroxyapatite ($Ca_{10}(PO_4)_6(OH)_2$), and other minor phases such as Ca phosphates, anhydrite ($CaSO_4$), various nitrates, and oxides and hydroxides of Ca, Mg, aluminium (Al), titanium (Ti), Mn, zinc (Zn) or Fe. Amorphous silica is of particular interest as it typically is in the form of phytoliths that contain and protect plant C from degradation (Wilding et al, 1967; Krull et al, 2003; Smith and White, 2004; Parr and Sullivan, 2005; Parr, 2006). Crystalline silica is also of interest because it has been found in some biochars where it poses a very high-level respiratory risk.

Morphologies and distribution patterns of minerals in several different biochars are shown in Figures 3.5 to 3.9. Figure 3.5 illustrates a range of morphologies, indicating that some of the mineral phases consist of more than one mineral type. Microprobe analysis of these biochars indicates that there is a large variation of mineral content even within each particle (see Figure 3.6). Figure 3.6 illustrates the distribution of both metals and non-metals in the end grain of a wood biochar. A variety of minerals can be identified that differ greatly between different biochars (see Figures 3.7 to 3.9).

Associated oils and their distribution

Most of the literature on bio-oils (e.g. Maggi and Delmon, 1994; Bridgwater and Boocock, 1997; Guan, 2004) relates to the compounds that are released when biomass is pyrolysed. Very little analysis has taken place of the organic molecules that remain on the surface.

Schnitzer et al (2007a, 2007b) carried out a detailed analysis of the residual bio-oils on biochars derived from the fast pyrolysis of chicken manure. They found that the individual compounds identified were grouped into the following six compound classes:

1 N-heterocyclics;
2 substituted furans;
3 phenol and substituted phenols;
4 benzene and substituted benzenes;
5 carbocyclics; and
6 aliphatics.

Prominent N-heterocyclics in bio-oil were methyl- and ethyl-substituted pyrroles, pyridines, pyrimidine, pyrazines and pteridine. The alkanes and alkenes ranged from *n*-C_7 to *n*-C_{18} and $C_{7:1}$ to $C_{18:1}$, respectively, and those in the biochar from *n*-C_7 to *n*-C_{19} and $C_{7:1}$ to $C_{19:1}$, respectively.

Some of these compounds (e.g. butenolide) have been found to be important in the germination of native species (Dixon, 1998); others have been identified as triggering the growth of microorganisms (sesquiterpenes) (Akiyama and Hayashi, 2006); and others have been found to have biocide properties (so-called smoke vinegar) (Guan, 2004).

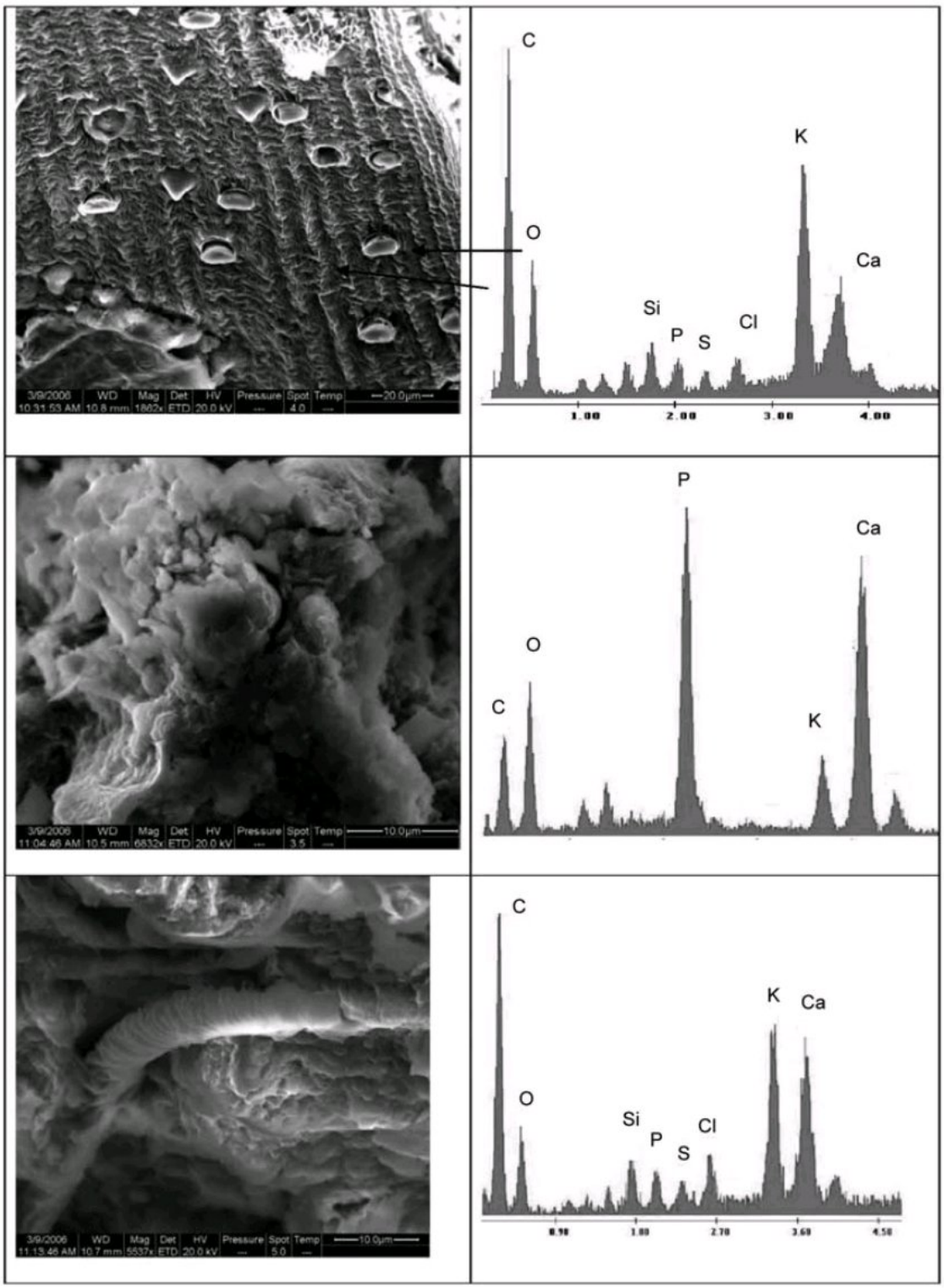

Figure 3.5 *Scanning electron microscopy (SEM) micrographs of different mineral phases in chicken manure biochar (produced at 450°C for 0.5hrs) and their energy-dispersive X-ray spectroscopy (EDS) spectra*

Note: biochar manufactured by BESTEnergies Pty.
Source: Electron Microscope Unit, University of NSW using a Quanta SEM

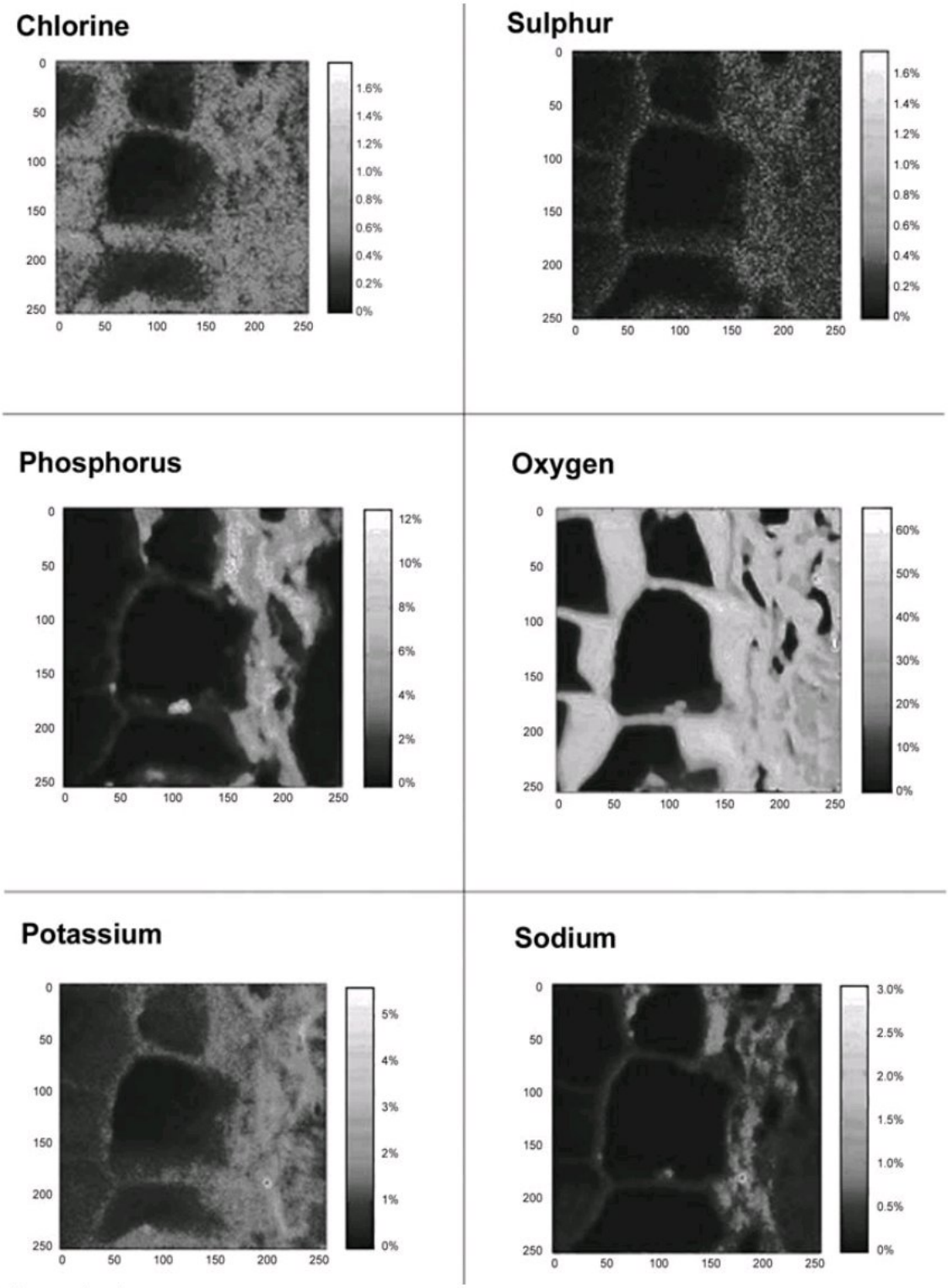

Note: all distances in microns

Figure 3.6 *Distribution of non-C elements on the surface of wood biochar (produced at 450°C for 0.5hrs) determined by microprobe analysis*

Note: biochar manufactured by BESTEnergies Pty.
Source: Electron Microscope Unit, University of NSW, Cameca, Japan

Surface chemistry

The surface chemistry of biochars, as expected from their heterogeneous compositions, is quite rich and varied. Biochar surfaces exhibit hydrophilic, hydrophobic, acidic and basic properties whose relative contributions to biochar reactivity depend upon the feedstock and on the thermal degradation process used to create the biochar. In this section we review the molecular properties that give rise to biochar surface chemistry and then discuss how these properties affect the ability of biochars to react with chemicals found in soil environments.

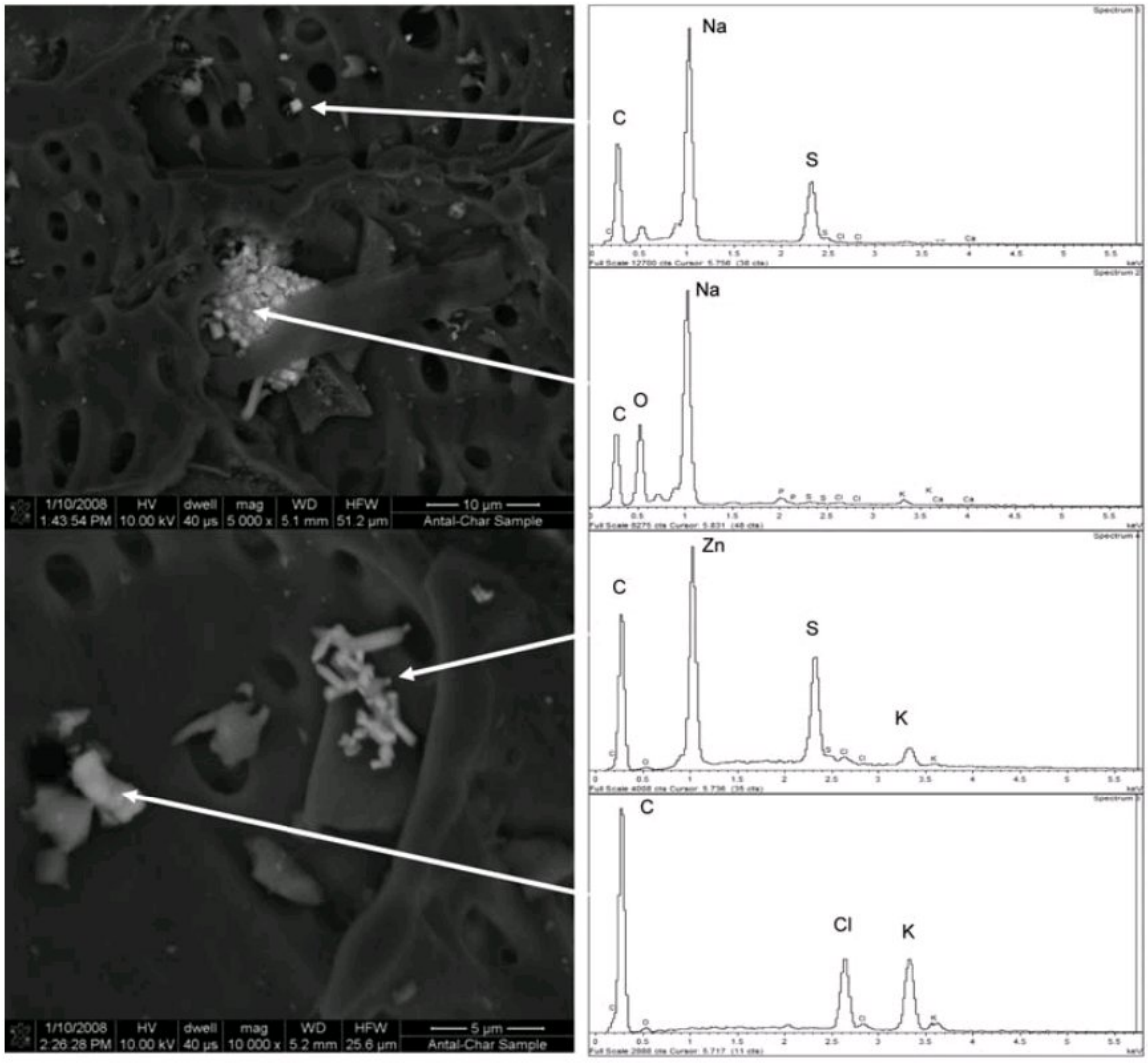

Figure 3.7 *SEM micrographs and associated EDS spectra for mineral phases in maize-cob biochar prepared by flash pyrolysis: probable minerals include (a) Na_2S; (b) Na_2O or Na_2CO_3; (c) ZnS; and (d) KCl*

Note: Operating conditions consisted of 2 to 20keV for SEM imaging and 20keV, 100 live seconds for the EDS analyses.

Source: Micrographs taken at the Environmental Molecular Sciences Laboratory, Richland, WA, using a Zeiss Leo 982 field emission-scanning electron microscope equipped with an Oxford INCA 300 EDS used for qualitative elemental analysis. Sample courtesy of Michael J. Antal, University of Hawaii.

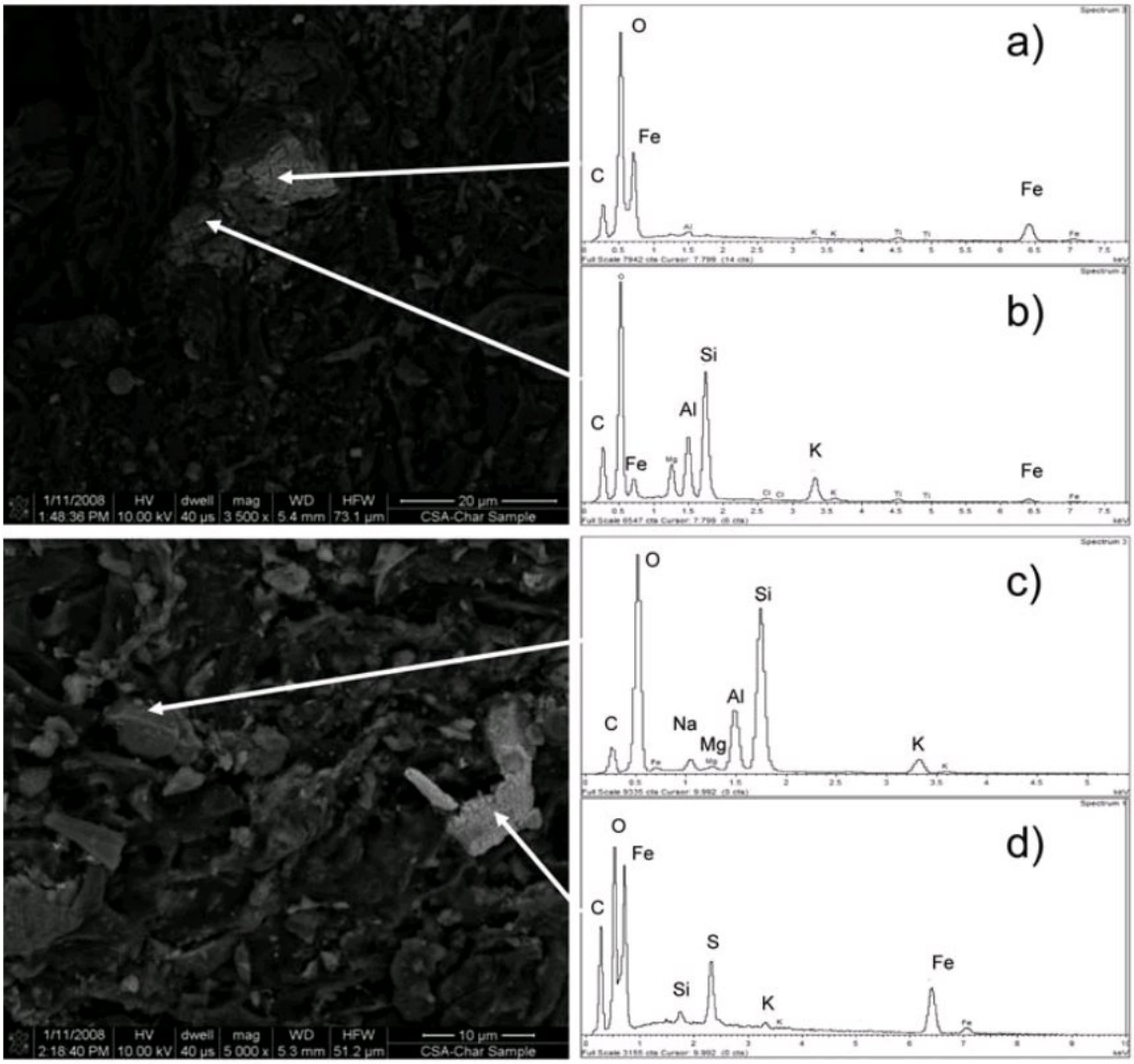

Figure 3.8 *SEM micrographs and associated EDS spectra for mineral phases in white oak biochar prepared by fast pyrolysis: probable minerals include (a) Fe_2O_3; (b) dehydroxylated layer silicate or a mixture of Si, Al, Mg and K oxides; (c) dehydroxylated layer silicate or a mixture of Si, Al and K oxides; and (d) FeS, $FeCO_3$, S, Fe_2O_3*

Source: Micrographs taken at the Environmental Molecular Sciences Laboratory, Richland, WA, as described in Figure 3.7. Sample courtesy of Stefan Czernik, National Renewable Energy Laboratory.

Carbon-based phases

Functional groups

Experimental evidence shows that a range of different functional groups exist on the surfaces of the graphene sheets (see Figure 3.10; Brennan et al, 2001). Hydrogen, O, N, P and S are incorporated in the aromatic rings as heteroatoms. Brennan et al (2001) state that the presence of heteroatoms results in surface chemical heterogeneity caused mainly by differences in the electronegativity of the heteroatoms relative to the C atoms. Groups such as OH, NH_2, OR or O(C=O)R are classified as electron donors (due to the presence of α or π electrons), whereas (C=O)OH, (C=O)H or NO_2 groups are classified as electron acceptors (due to the

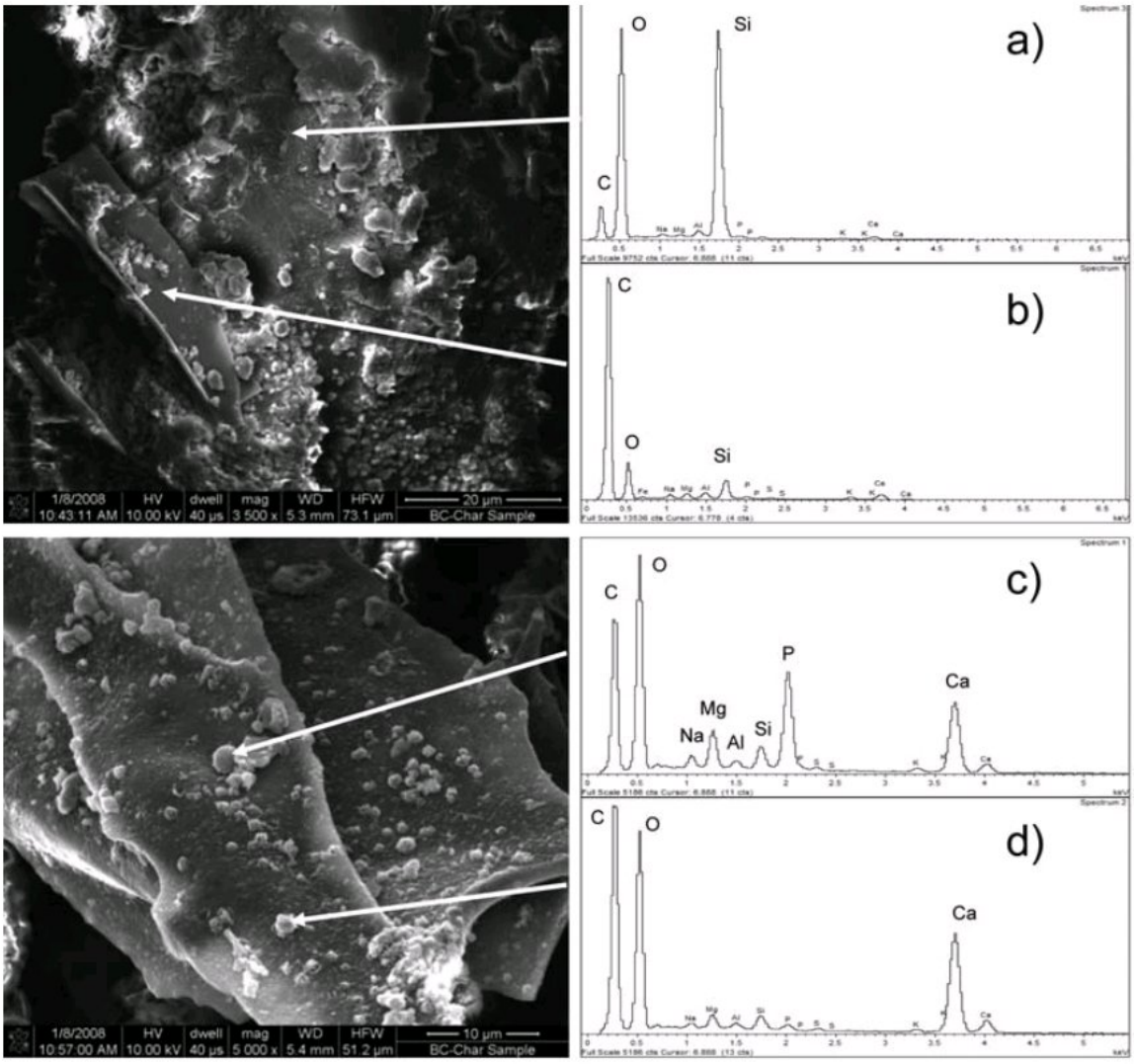

Figure 3.9 *SEM micrographs and associated EDS spectra for mineral phases in poplar wood biochar from a combustion facility: probable minerals include (a) amorphous SiO_2; (b) trace dehydroxylated silicates (mostly char); (c) $Ca_{10}(PO_4)_6(OH)_2$, $CaHPO_4$; and (d) CaO, $CaCO_3$*

Source: micrographs taken at the Environmental Molecular Sciences Laboratory, Richland, WA, as described in Figure 3.7

presence of empty orbitals). Carboxyl groups are strong Brønsted acids. Less acidic groups include phenols and carbonyls. Chromenes and pyrones are basic functional groups.

As demonstrated in Figures 3.7 to 3.9, there are very large differences in mineral matter content and composition on the surfaces of biochars. This difference is manifested at a level measured in micrometres. Thus, acidic and basic sites may coexist within micrometres of each other on the outer surfaces and pores of the particle.

In high-mineral ash biochars, it is probable that some of the functional groups will contain metals. Schnitzer et al (2007a) and Koutcheiko et al (2007) detected a range of different N- and S-based functional groups in chicken manure biochar. Data from various studies (e.g. Elizalde-Gonzalez et al, 2007) indicate that the relative concentration of each of the functional groups depends upon initial composition of the biomass, final

reaction temperature, composition of the gas surrounding the charring particle (at the final reaction temperature), rate of heating and any post-treatment.

Operational determination of acidic and basic functional groups on biochars can be performed by Boehm titrations (Boehm, 1994) in which the biochar is equilibrated in the presence of successively stronger bases (HCO_3^-, CO_3^{2-}, OH^-, ethoxide) or a strong acid, followed by titration of the extract with strong acid or base to determine the fraction that reacted. Differences in the amounts of acid or base needed are used to estimate the relative amounts of carboxylic, lactonic, phenolic and carbonylic functional groups (base equilibrations) or basic functionalities (acid equilibration). For characterization of biochars used as soil amendments, the ethoxide equilibration is commonly omitted as it measures functional groups that are dissociated only at very high pH.

The Boehm titration works well for hydrophilic biochars, but encounters difficulties when significant amounts of bio-oil or mineral surfaces are present. In these circumstances, analysis by spectroscopic means may be helpful. X-ray photoelectron spectroscopy (XPS) and electron energy loss spectroscopy (EELS) can both provide information about the types of functional groups present. For example, Cohen-Ofri et al (2007) used EELS to show the incorporation of O groups into ancient biochars as part of the aging process. Cheng et al (2008) used C1s XPS in a similar manner to follow oxidation of C in biochar from soils at charcoal production sites in eastern North America.

Oxygen

Biochar reacts readily with atmospheric O_2 to yield O-containing functional groups at the surface (Shafizadeh, 1982; Bourke et al, 2007). Carbon-O groups are also formed from reaction with oxidizing gases such as ozone, nitric oxide and CO_2, as well as reactions with oxidizing solutions (Marsh et al, 1997). Swiatkowski et al (2004) note that pyrone sites may be the result of the adsorption of molecular O in the form of superoxide ions O_{2-} and the dissociatively adsorbed O, such as O^- or O^{2-}.

Nitrogen and sulphur

In biochars derived from manures, sewage sludge and rendering wastes, N and S functional groups will be more abundant than in lignocellulosic biochars. Areas of high N are

Table 3.2 *Summary of functional groups of S and N in a chicken-manure biochar (within the accuracy of XPS, pyridone-N cannot be distinguished from pyrrole-N)*

Sample	*Peak*	*Functional groups*	*Binding energy (eV)*	*Content (percentage of total signal)*
Raw biochar	N 1s	Pyridinic	398.4–398.8	31
		Pyrrolic or pyridonic, amine	399.4–400.5	69
		Quaternary N	≥401.4	–
	S 2p	Thiophenic, sulphidic, pyrite	163.7–164.6	31
		Sulphonic and sulphates	≥168.0	69
Activated carbon 800°C, CO_2	N 1s	Pyridinic	398.4–398.8	39
		Pyrrolic or or pyridonic[a]	399.8–400.3	24
		Quaternary N	≥401.4	37
	S 2p	Thiophenic, sulphidic	164.3–165.5	100

Source: Koutcheiko et al (2007)

centres for high basicity. Koutcheiko et al (2007) prepared chicken manure biochar by heating to 360°C in a fast pyrolyis unit (no reaction time was reported). The biochar was then heated to 800°C and activated with CO_2. The main functional groups containing N for the low temperature biochar (as measured by XPS) were pyrrolic or pyridinic amines, whereas the high temperature biochars had nearly equal amounts of pyridinic and quaternary groups (see Table 3.2). Bagreev et al (2001) noted a similar trend when examining changes in sewage sludge biochars made at 450°C to 900°C in a fixed-bed reactor. At the lower temperatures, they detected amine functionalities by diffuse-reflectance infared spectroscopy, and at higher temperatures the same analysis suggested that the organic N was incorporated within the biochar as pyridine-like compounds.

Koutcheiko et al (2007) also identified S functional groups in their chicken manure biochar. In the low-temperature biochar, the main S functional groups were sulphonates and sulphates, whereas thiophene and sulphide groups predominated in the high-temperature biochar (see Table 3.2). Knudsen et al (2004) noted that in wheat straw biochar, the S remains as a sulphate until approximately 500°C, at which temperature it starts to transform to an insoluble sulphide (e.g. CaS, K_2S) in the biochar matrix, or from fixed to reactive biochar surfaces by either the addition of S to unsaturated sites or the substitution of O in surface oxides (Knudsen et al, 2004). These forms of S are expected to be water insoluble and biologically less available.

Mineral phases

A priori, one would expect that the functional groups on the surfaces of entrained mineral phases are similar to those of 'free' mineral phases not associated with biochar.

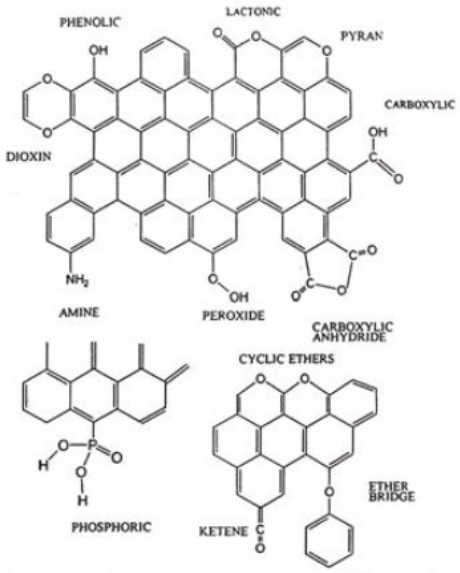

Figure 3.10 *Heteroatoms and functional groups commonly found in activated carbons*

Source: reprinted from Brennan et al (2001) with permission from Elsevier

Specifically, amphoteric sites (sites which react as both an acid and a base) exist on oxide surfaces whose surface charge varies with solution pH. Thus, under acidic conditions, the surfaces tend to be positively charged, and under alkaline conditions, negatively charged. The basal surfaces (and internal galleries) of layer silicates offer a permanently charged site that is negatively charged, in addition to edge sites that are amphoteric. However, many layer silicates that might have been present in the original biomass are irreversibly altered by dehydroxylation processes when thermal degradation temperatures exceed 500°C, and thus are transformed to oxides. The surfaces of carbonate minerals, in general, behave similarly to oxides due to the presence of O in the carbonate anion. Sulphide minerals, on the other hand, exhibit a significant range in behaviour when exposed to aqueous solutions, with the S atom at the surface eventually releasing seven electrons as the mineral surface is oxidized by water or other

dissolved oxidants (Rimstidt and Vaughan, 2003). Thus, charge on the surface of the sulphide may range from negative to neutral to positive depending upon the oxidation state of S. With increasing oxidation, as one might expect, the surface properties of the sulphide mineral approach those of oxide minerals. An in-depth discussion of charge development on oxide and related mineral surfaces is beyond the scope of this chapter. The interested reader may wish to consult geochemical texts such as Stumm and Morgan (1996), Langmuir (1997) and Essington (2003).

Influence of surface properties on sorption

The various functional groups on the surfaces of biochar influence sorption by the nature of their surface charge and by the availability of π electrons. As with oxide surfaces, the charge on the functional groups may change depending upon the pH of the solution (i.e. the surface is amphoteric), thus affecting sorption behaviour. Examples of these changes and the associated functional groups are shown in Figure 3.11 and discussed in great detail by Radovic et al (2001). Not surprisingly, the nature of the sorbate also affects its ability to sorb. Non-transition metals, for example, are sorbed strictly by electrostatic forces, whereas transition metals with their exposed π-orbitals can bond with π electrons in the plane of the graphene sheets in addition to electrostatic bonding at oxidized sites on the edges of the graphene sheets. Many of these metals are also amphoteric, making a description of their sorption behaviour even more complicated. With transition metals, at least some sorption will occur simply by the π-electron mechanism if electrostatic repulsion forces can be overcome. In their work on Pb^{2+} sorption, Swiatkowski et al (2004) listed the various ways in which metals can be adsorbed on biochar. We show them here for a generic divalent metal cation indicated as Me^{2+}:

Lewis base reaction:

$$\geqslant C{:}H_3O^+ + MeOH^+ \Leftrightarrow \geqslant C{:}MeOH^+ + H_3O^+$$

Cπ-cation interaction:

$$\geqslant C{:} + Me^{2+} \Leftrightarrow \geqslant C{:}Me^{2+}$$

For basic sites:

$$\begin{aligned}
&\geqslant C\text{-}OH + Me^{2+} + 3H_2O \Leftrightarrow \geqslant COMeOH + 2H_3O^+\\
&\geqslant C\text{-}O^{-*} + Me^{2+} + 2H_2O \Leftrightarrow \geqslant C\text{-}O\text{–}MeOH + H_3O^+\\
&\geqslant N{:} + Me^{2+} + 2H_2O \Leftrightarrow \geqslant N\text{-}MeOH^+ + H_3O^+.
\end{aligned}$$

For oxidized acidic sites:

$$\begin{aligned}
&\geqslant C\text{-}COOH + Me^{2+} + H_2O \Leftrightarrow \geqslant C\text{-}COOMe^+ + H_3O^+\\
&(\geqslant C\text{-}COOH)_2 + Me^{2+} + 2H_2O \Leftrightarrow (\geqslant C\text{-}COO)_2Me + 2H_3O^+\\
&\geqslant C\text{-}OH + Me^{2+} + H_2O \Leftrightarrow \geqslant C\text{-}OMe^+ + H_3O^+
\end{aligned}$$

Many organic sorbates, such as phenols, anilines and other functionalized aromatic molecules, also exhibit amphoteric behaviour and, like the amphoteric transition metals, must strike a balance between electrostatic and π-electron sorption mechanisms. In general, these molecules tend to sorb most strongly at solution pH values near their points of zero charge (Radovic et al, 2001). Recent work by Chen et al (2008), Nguyen et al (2007) and by Pignatello and co-workers (Braida et al, 2003; Sander and Pignatello, 2005, 2007; Zhu and Pignatello, 2005, Zhu et al, 2005, Pignatello et al, 2006) offers many insights into the sorption behaviour of aromatic molecules on biochar surfaces.

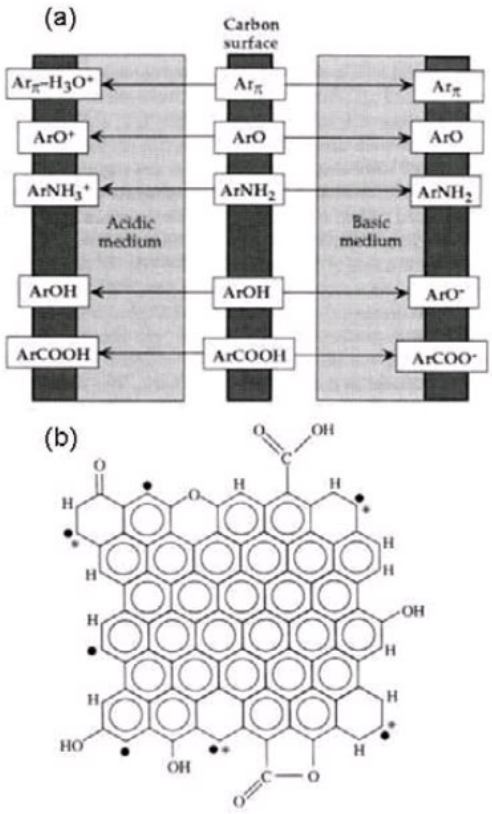

Figure 3.11 *(a) Macroscopic representation of the features of C surface chemistry thought to be sufficient for understanding aqueous-phase sorption phenomena; (b) microscopic representation of the functional groups thought to be sufficient for understanding aqueous-phase adsorption phenomena*

Notes: (a) Ar = aromatic. (b) • Represents an unpaired sigma electron; •* represents an in-plane sigma pair; * represents a localized π electron.

Source: reprinted from Radovic et al (2001) with permission from Elsevier

References

Akiyama, K. and Hayashi, H. (2006) 'Strigolactones: Chemical signals for fungal symbionts and parasitic weeds in plant roots', *Annals of Botany*, vol 97, pp925–931

Antal, M. J. Jr. and Grønli, M. (2003) 'The art, science, and technology of charcoal production', *Industrial and Engineering Chemistry Research*, vol 42, pp1619–1640

Antal, M. J. Jr., Allen, S. G., Dai, X.-F., Shimizu, B., Tam, M. S. and Grønli, M. (2000) 'Attainment of the theoretical yield of carbon from biomass', *Industrial and Engineering Chemistry Research*, vol 39, pp4024–4031

Bagreev, A., Bandosz, T. J. and Locke, D. C. (2001) 'Pore structure and surface chemistry of adsorbents obtained by pyrolysis of sewage sludge-derived fertilizer', *Carbon*, vol 39, pp1971–1977

Bergman, P. C. A. and Kiel, J. H. A. (2005) 'Torrefaction for biomass upgrading', www.ecn.nl/docs/library/report/2005/rx05180.pdf, accessed 1 August 2008

Boehm, H. P. (1994) 'Some aspects of the surface chemistry of carbon blacks and other carbons', *Carbon*, vol 32, pp759–769

Bourke, J. (2006) *Preparation and Properties of Natural, Demineralized, Pure, and Doped Carbons from Biomass; Model of the Chemical Structure of Carbonized Charcoal*, MS thesis, The University of Waikato, New Zealand

Bourke, J., Manley-Harris, M., Fushimi, C., Dowaki, K., Nunoura, T. and Antal, M. J. Jr., (2007) 'Do all carbonized charcoals have the same chemical structure? 2. A model of the chemical structure of carbonized charcoal', *Industrial and Engineering Chemistry Research*, vol 46, pp5954–5967

Bradbury, A. G. W. and Shafizadeh, F. (1980) 'Chemisorption of oxygen on cellulose char', *Carbon*, vol 18, pp109–116

Braida, W. J., Pignatello, J. J., Lu, Y., Ravikovitch, P., Neimark, A. V. and Xing, B. (2003) 'Sorption hysteresis of benzene in charcoal particles', *Environmental Science and Technology*, vol 37,

pp409–417
Brennan, J. K., Bandosz, T. J., Thomson, K. T. and Gubbins, K. E. (2001) 'Water in porous carbons', *Colloids and Surfaces A: Physicochemical and Engineering Aspects*, vol 187–188, pp539–568
Bridgwater, A. V. and Boocock, D. G. B. (eds) (1997) *Developments in Thermochemical Biomass Conversion*, Blackie Academic and Professional, London, UK
Bridgwater, A. and Boocock, D. G. B. (2006) *Science in Thermal and Chemical Biomass Conversion*, CPL Press, Newbury, UK
Chen, B., Zhou, D. and Zhu, L. Z. (2008) 'Transitional adsorption and partition of nonpolar and polar aromatic contaminants by biochars of pine needles with different pyrolytic temperatures', *Environmental Science and Technology*, vol 42, pp5137–5143
Cheng, C.-H., Lehmann, J. and Engelhard, M. H. (2008) 'Natural oxidation of black carbon in soils: Changes in molecular form and surface charge along a climosequence', *Geochimica et Cosmochimica Acta*, vol 72, pp1598–1610
Cohen-Ofri, I., Weiner, L., Boaretto, E., Mintz, G. and Weiner, S. (2006) 'Modern and fossil charcoal: Aspects of structure and diagenesis', *Journal of Archaeological Science*, vol 33, pp428–439
Cohen-Ofri, I., Popovitz-Biro, R. and Weiner, S. (2007) 'Structural characterization of modern and fossilized charcoal produced in natural fires as determined by using electron energy loss spectroscopy', *Chemistry, A European Journal*, vol 13, pp2306–2310
Cui, X. J., Antonietti, M. and Yu, S. H. (2006) 'Structural effects of iron oxide nanoparticles and iron ions on the hydrothermal carbonization of starch and rice carbohydrates', *Small*, vol 2, pp756–759
Degroot, W. F. and Shafizadeh, F. (1983) 'Influence of inorganic additives on oxygen chemisorption on cellulosic chars', *Carbon*, vol 21, pp61–67
Demirbas, A. (2001) 'Carbonization ranking of selected biomass for charcoal, liquid and gaseous products', *Energy Conversion and Management*, vol 42, pp1229–1238
Dixon, K. (1998) *Smoke Germination of Australian Plants*, RIRDC report (98/108, KPW–1A), Kings Park and Botanic Garden Plant Science Division, Perth, Australia
Edye, L. A., Richards, G. N. and Zheng, G. (1993) 'Transition metals as catalysts for pyrolysis and gasification of biomass', in M. R. Khan (ed) *Clean Energy from Waste and Coal*, American Chemical Society Symposium Series 515, American Chemical Society, Washington, DC, pp90–103
Elizalde-Gonzalez, M. P., Mattusch, J., Pelaez-Cid, A. A. and Wennrich, R. (2007) 'Characterization of adsorbent materials prepared from avocado kernel seeds: Natural, activated and carbonized forms', *Journal of Analytical and Applied Pyrolysis*, vol 78, pp185–193
Essington, M. E. (2003) *Soil and Water Chemistry: An Integrative Approach*, CRC Press, Boca Raton, FL
Feng, J.-W., Zheng, S. and Maciel, G. E. (2004) 'EPR investigations of the effects of inorganic additives on the charring and char/air interactions of cellulose,' *Energy and Fuels*, vol 18, pp1049–1065
Figueiredo, J. L., Valenzuela, C., Bernalte, A. and Encinar, J. M. (1989) 'Pyrolysis of holm-oak wood: Influence of temperature and particle size', *Fuel*, vol 68, pp1012–1017
Franklin, R. E. (1951) 'Crystallite growth in graphitizing and non-graphitizing carbons', *Proceedings of the Royal Society of London, Series A, Mathematical and Physical Sciences*, vol 209, pp196–218
Guan, M. (2004) *Manual for Bamboo Charcoal Production and Utilization*, Bamboo Engineering Research Center, Nanjing Forestry University, China
Kercher, A. K. and Nagle, D. C. (2003) 'Microstructural evolution during charcoal carbonization by X-ray diffraction analysis', *Carbon*, vol 41, pp15–27
Knudsen, J. N., Jensen, P. A., Lin, W., Frandsen, F. J. and Dam-Johnson, K. (2004) 'Sulfur transformations during thermal conversion of herbaceous biomass', *Energy and Fuels*, vol 18, pp810–819
Koutcheiko, S., Monreal, C.M., Kodama, H., McCracken, T. and Kotlyar, L. (2007) 'Preparation and characterization of activated carbon derived from the thermo-chemical conversion of chicken manure', *Bioresource Technology*, vol 98, pp2459–2464

Krull, E. S., Skjemstad, J. O., Graetz, D., Grice, K., Dunning, W., Cook, G. D. and Parr, J. F. (2003) '^{13}C-depleted charcoal from C3 and C4 grasses and the role of occluded carbon in phytoliths', *Organic Geochemistry*, vol 34, pp1337–1352

Langmuir, D. (1997) *Aqueous Environmental Geochemistry*, Prentice-Hall, Upper Saddle River, NJ

Lima, I. M. and Marshall, W.E. (2005) 'Granular activated carbons from broiler manure: Physical, chemical and adsorptive properties', *Bioresource Technology*, vol 96, pp699–706

Maggi, R. and Delmon, B. (1994) 'Comparison between "slow" and "flash" pyrolysis oils from biomass', *Fuel*, vol 73, no 5, pp671–677

Marschner, H. (1995) *The Mineral Nutrition of Higher Plants*, Academic Press, San Diego, CA

Marsh, H., Heintz, E. A. and Rodriguez-Reinoso, F. (1997) *Introduction to Carbon Technologies*, University of Alicante, Alicante, Spain

Nguyen, T. H., Cho, H. H., Poster, D. L. and Ball, W. P. (2007) 'Evidence for a pore-filling mechanism in the adsorption of aromatic hydrocarbons to a natural wood char', *Environmental Science and Technology*, vol 41, pp1212–1217

Paris, O., Zollfrank, C. and Zickler, G. A. (2005) Decomposition and carbonisation of wood biopolymers – a microstructural study of softwood pyrolysis', *Carbon*, vol 43, pp53–66

Parr, J. F. (2006) 'Effect of fire on phytolith coloration', *Geoarchaelogy – An International Journal*, vol 21, pp171–185

Parr, J. F. and Sullivan, L. A. (2005) 'Soil carbon sequestration in phytoliths', *Soil Biology and Biochemistry*, vol 37, pp117–124

Pignatello, J. J., Kwon, S. and Lu, Y. (2006) 'Effect of natural organic substances on the surface adsorptive properties of environmental black carbon (char): Attenuation of surface activity by humic and fulvic acids', *Environmental Science and Technology*, vol 40, pp7757–7763

Purevsuren, B., Avida, B., Gerelmaa, T., Davaajava, Y., Morgan, T. J., Herod, A. A. and Kandiyoti, R. (2004) 'The characterisation of tar from the pyrolysis of animal bones', *Fuel*, vol 83, pp799–805

Radovic, L. R., Moreno-Castilla, C. and Rivera-Utrilla, J. (2001) 'Carbon materials as adsorbents in aqueous solutions', *Chemistry and Physics of Carbon: A Series of Advances*, vol 27, pp227–405

Raveendran, K., Ganesh, A. and Khilart, K. C. (1995) 'Influence of mineral matter on biomass pyrolysis characteristics', *Fuel*, vol 74, pp1812–1822

Rimstidt, J. D. and Vaughan, D. J. (2003) 'Pyrite oxidation: A state-of-the-art assessment of the reaction mechanism', *Geochimica et Cosmochimica Acta*, vol 67, pp873–880

Rothlein, B. (2006) 'Magic coal from the steam cooker', *Max Planck Research*, vol 3, pp20–25

Sander, M. and Pignatello, J. J. (2005) 'Characterization of charcoal adsorption sites for aromatic compounds: Insights drawn from single-solute and bi-solute competitive experiments', *Environmental Science and Technology*, vol 39, pp1606–1615

Sander, M. and Pignatello, J. J. (2007) 'On the reversibility of sorption to black carbon: Distinguishing true hysteresis from artificial hysteresis caused by dilution of a competing adsorbate', *Environmental Science and Technology*, vol 41, pp843–849

Schenkel, Y. (1999) *Modelisation des Flux Massiques et Energetiques dans la Carbonisation du Bois en Four Cornue*, PhD thesis, Université des Sciences Agronomiques de Gembloux, Gembloux, Belgium

Schnitzer, M. I., Monreal, C. M., Facey, G. A and Fransham, P. B. (2007a) 'The conversion of chicken manure to biooil by fast pyrolysis I. Analyses of chicken manure, biooils and char by C-13 and H-1 NMR and FTIR spectrophotometry', *Journal of Environmental Science and Health B*, vol 42, pp71–77

Schnitzer, M. I., Monreal, C. M., Jandl, G. and Leinweber, P. (2007b) 'The conversion of chicken manure to biooil by fast pyrolysis II. Analysis of chicken manure, biooils, and char by curie-point pyrolysis-gas chromatography/mass spectrometry (Cp Py-GC/MS)', *Journal of Environmental Science and Health B*, vol 42, pp79–95

Scott, D. S., Piskorz, J., Bergougnou, M. A., Graham, R. and Overend, R. P. (1988) 'The role of temperature in the fast pyrolysis of cellulose and wood', *Industrial and Engineering Chemistry Research*, vol 27, pp8–15

Shafizadeh, F. (1982) 'Introduction to pyrolysis of biomass', *Journal of Analytical and Applied*

Pyrolysis, vol 3, pp283–305

Skodras, G., Grammelis, P., Basinas, P., Kakaras, E. and Sakellaropoulos, G. (2006) 'Pyrolysis and combustion characteristics of biomass and waste-derived feedstock', *Industrial and Engineering Chemistry Research*, vol 45, pp3791–3799

Smith, F. A. and White, J. W. C. (2004) 'Modern calibration of phytolith carbon isotope signatures for C3/C4 paleograssland reconstruction', *Palaeogeography, Palaeoclimatology, Palaeoecology*, vol 207, pp277–304

Stresov, V., Patterson, M., Zymla, V., Fisher, K., Evans, T. J. and Nelson, P. F. (2007) 'Fundamental aspects of biomass carbonisation', *Journal of Analytical and Applied Pyrolysis*, vol 79, pp91–100

Stumm, W. and Morgan, J. J. (1996) *Aquatic Chemistry: Chemical Equilibria and Rates in Natural Waters*, third edition, Wiley-Interscience, New York, NY

Swiatkowski, A., Pakula, B., Biniak, S. and Walczyk, M. (2004) 'Influence of the surface chemistry of modified activated carbon on its electrochemical behaviour in the presence of lead(II) ions', *Carbon*, vol 42, pp3057–3069

Titirici, M. M., Thomas, A., Yu, S. H., Muller, J. O. and Antonietti, M. (2007a) 'A direct synthesis of mesoporous carbons with bicontinuous pore morphology from crude plant material by hydrothermal carbonization', *Chemistry of Materials*, vol 19, pp4205–4212

Titirici, M. M., Thomas, A. and Antonietti, M. (2007b) 'Back in the black: Hydrothermal carbonization of plant material as an efficient chemical process to treat the CO_2 problem?', *New Journal of Chemistry*, vol 31, pp787–789

Tito Ferro, D., Torres, A., Beaton Soler, P. and Zanzi, R. (2004) 'Biomass torrefaction', in W. P. M. Van Swaaij, T. Fjällström, P. Helm and A. Grassi (eds) *2nd World Conference and Technology Exhibition on Biomass for Energy, Industry and Climate Protection*, 10–14 May 2004, Palazzo dei Congressi, Rome, Italy, ETA–Florence and WIP–Munich, pp859–862, http://hem.fyristorg.com/zanzi/paper/zanziV2A–17.pdf, accessed 1 August 2008

Varhegyi, G., Jakab, E. and Antal, M. J. (1994) 'Is the Broido–Shafizadeh model for cellulose pyrolysis true?', *Energy Fuels*, vol 8, p1345

Wilding, L. P., Brown, R. E. and Holowaychuk, N. (1967) 'Accessibility and properties of occluded carbon in biogenic opal', *Soil Science*, vol 103, pp56–61

Wornat, M. J., Hurt, R. H. and Yang, N. Y. C. (1995) 'Structural and compositional transformations of biomass chars during combustion', *Combustion Flame*, vol 100, pp131–143

Yu, C., Tang. Y., Fang, M., Luo, Z. and Cen, K. (2005) 'Experimental study on alkali emission during rice straw pyrolysis', *Journal of Zhejiang University (Engineering Science)*, vol 39, pp1435–1444

Zhu, D. and Pignatello, J. J. (2005) 'Characterization of aromatic compound sorptive interactions with black carbon (charcoal) assisted by graphite as a model', *Environmental Science and Technology*, vol 39, pp2033–2041

Zhu, D., Kwon, S. and Pignatello, J. J. (2005) 'Adsorption of single-ring organic compounds to wood charcoals prepared under different thermochemical conditions', *Environmental Science and Technology*, vol 39, pp3990–3998